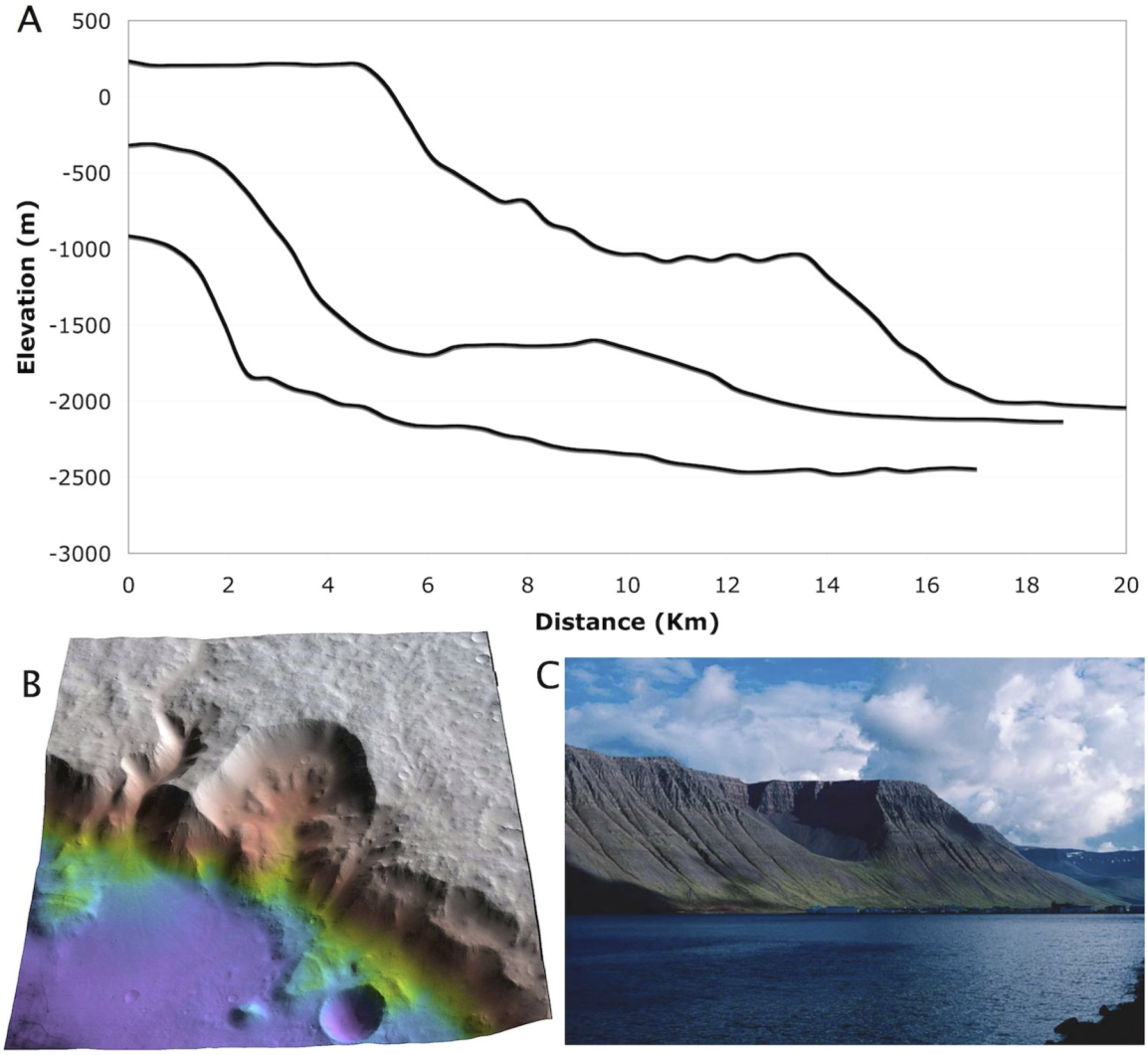

Figure DR1. A. Elevation profiles along cirque valleys in the Aeolis Mensae region. B. 3-D DEM of a cirque valley dissecting the topographic dichotomy. C. Example of a trough-side cirque eroded into the basalt plateau above Isafjordur, northwest Iceland. From Evans (2007).

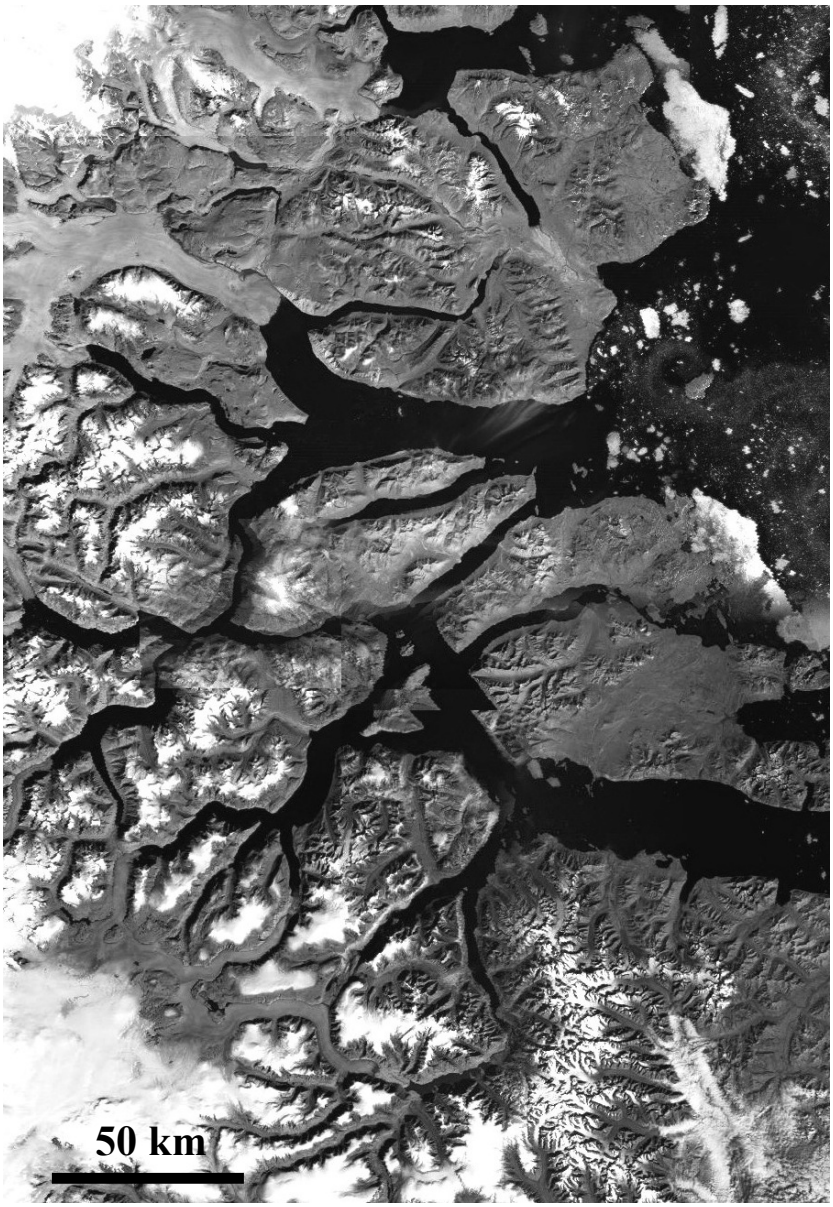

Figure DR2. Image mosaic of the East coast of Greenland as a possible analogue of the Martian fretted terrains. Credit: USGS

Regional context

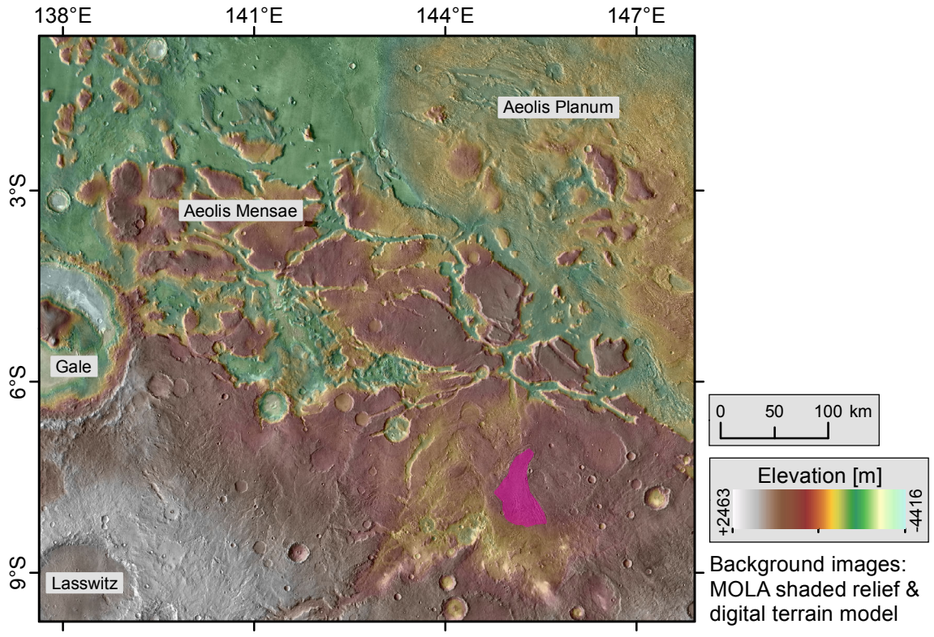

Crater counting area **1**

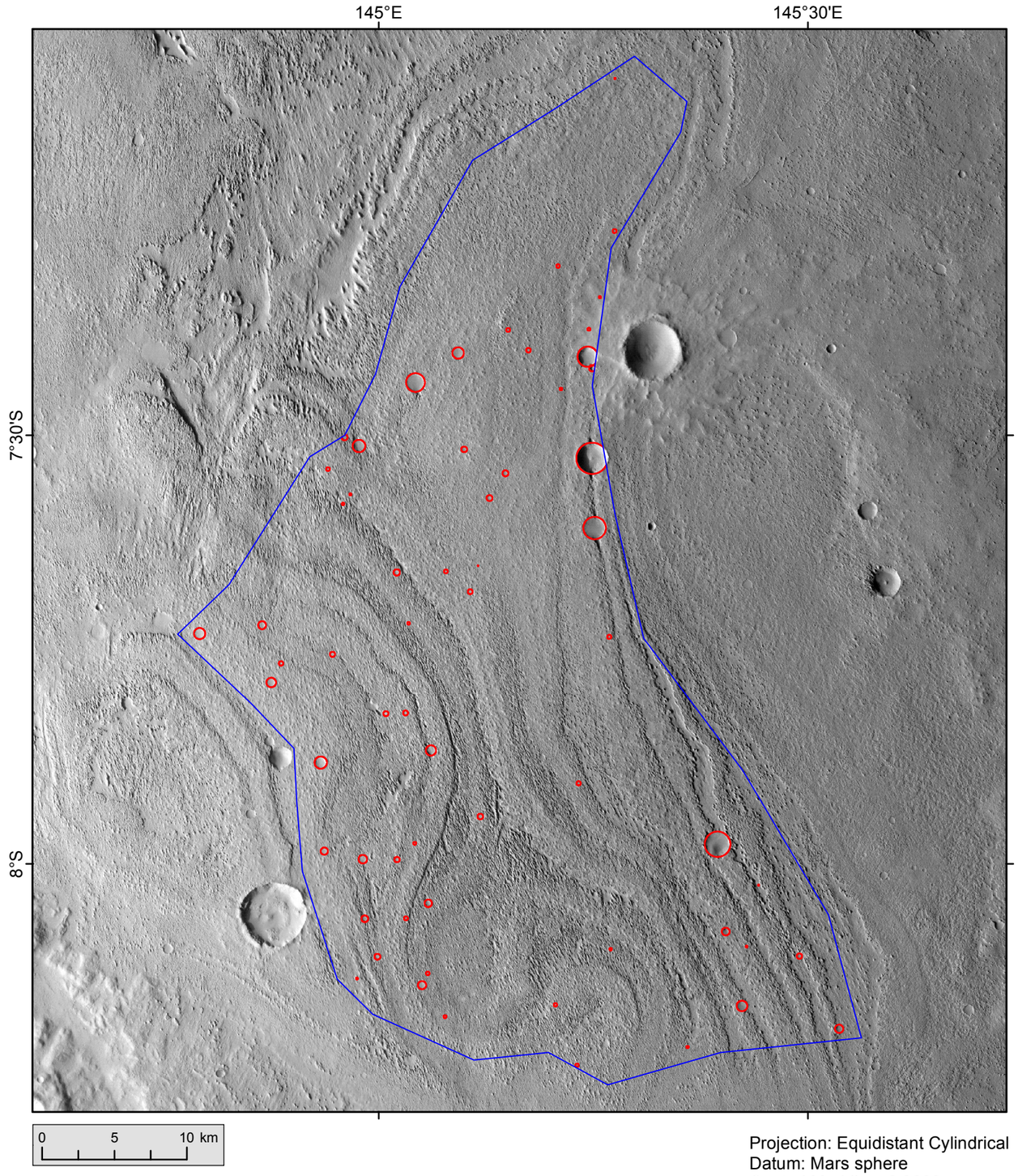

Projection: Equidistant Cylindrical
Datum: Mars sphere
Central Meridian: 0.0000
Standard Parallel 1: 0.0000
Units: Meter

Crater model age(s)

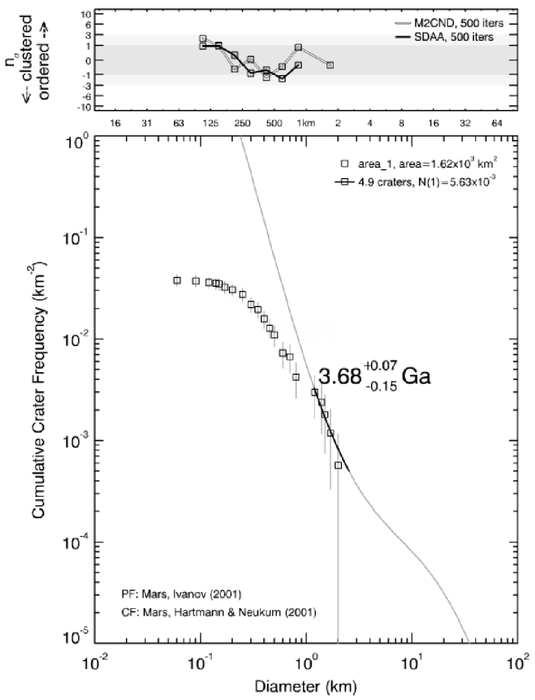

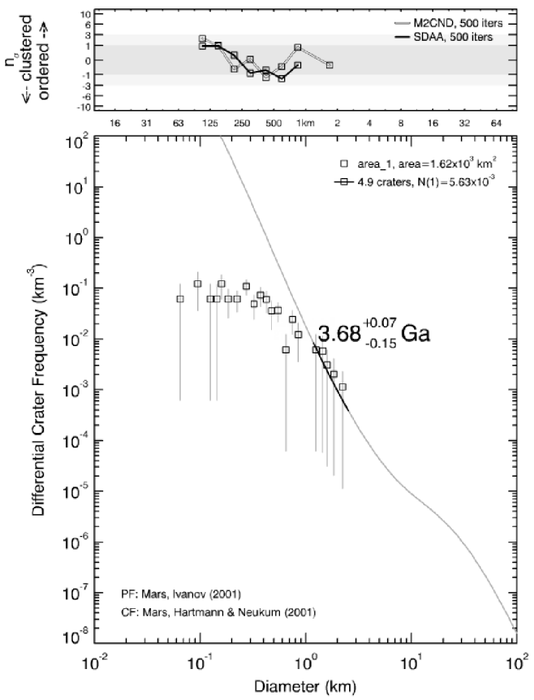

Regional context

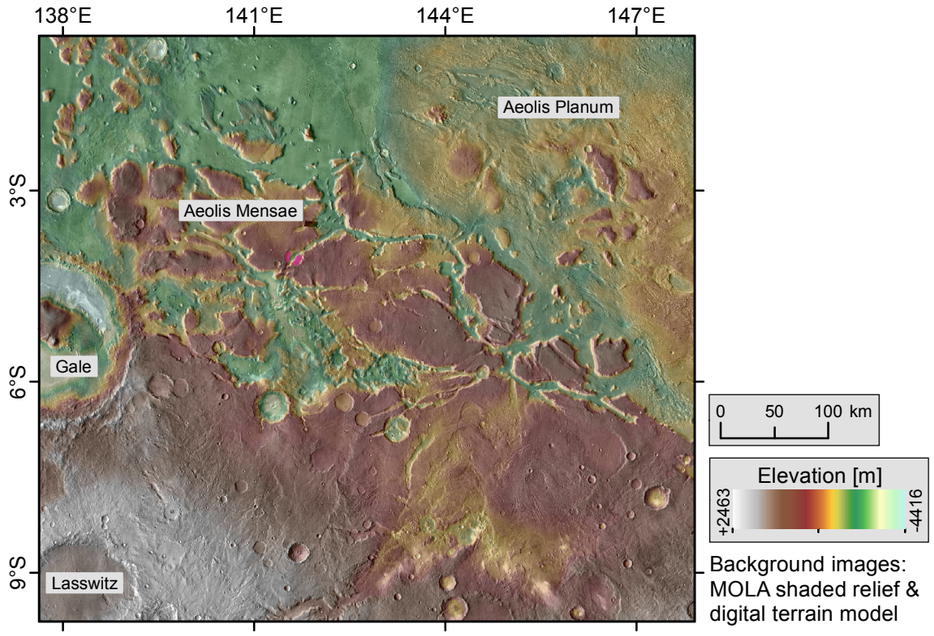

Crater counting area **2**

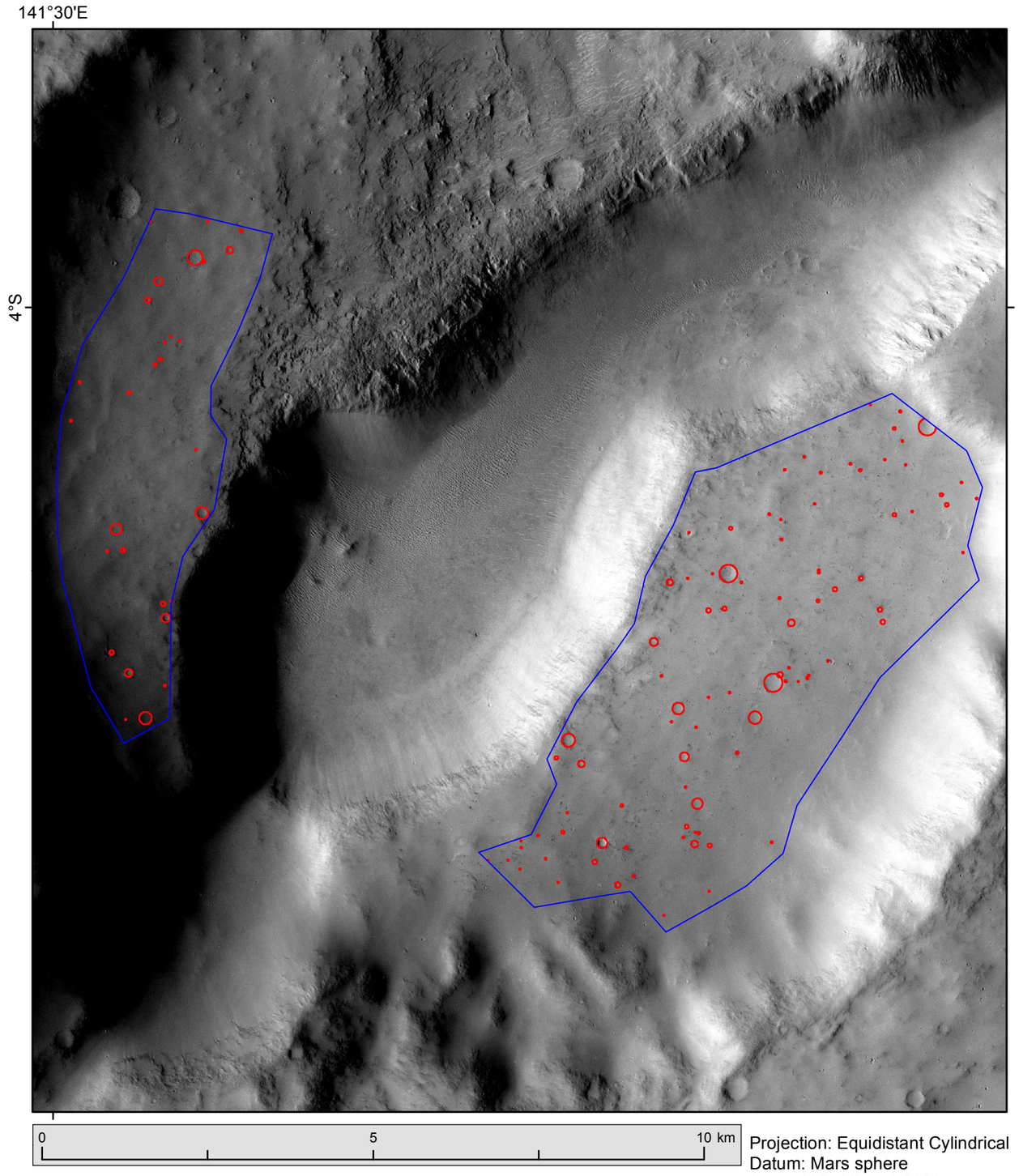

Crater model age(s)

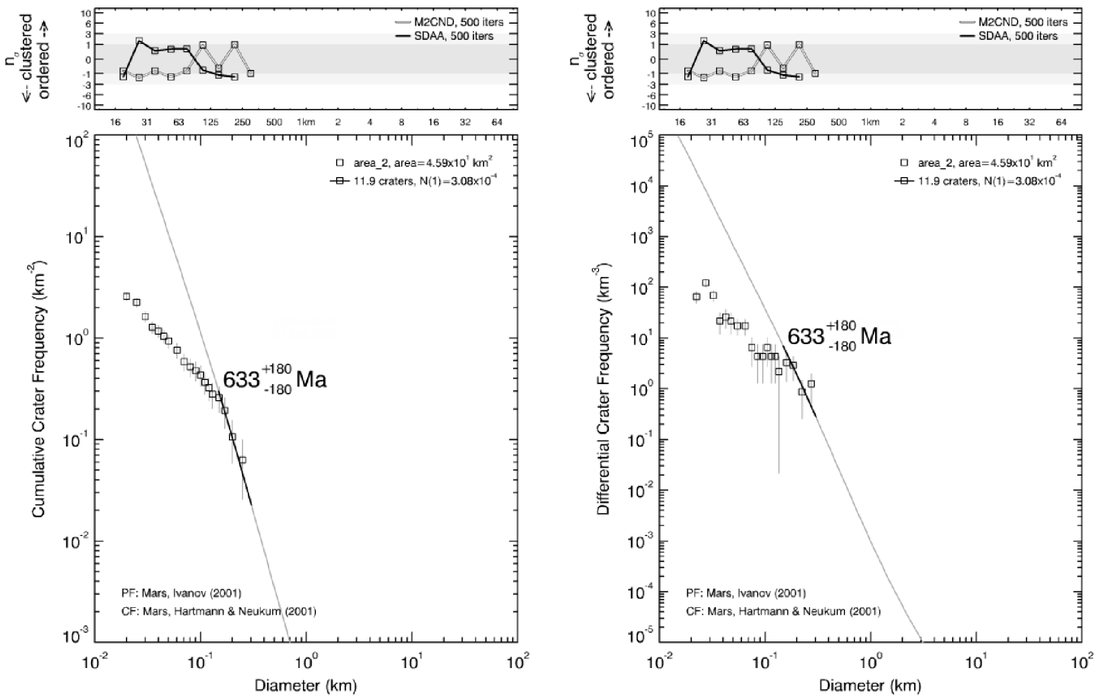

Regional context

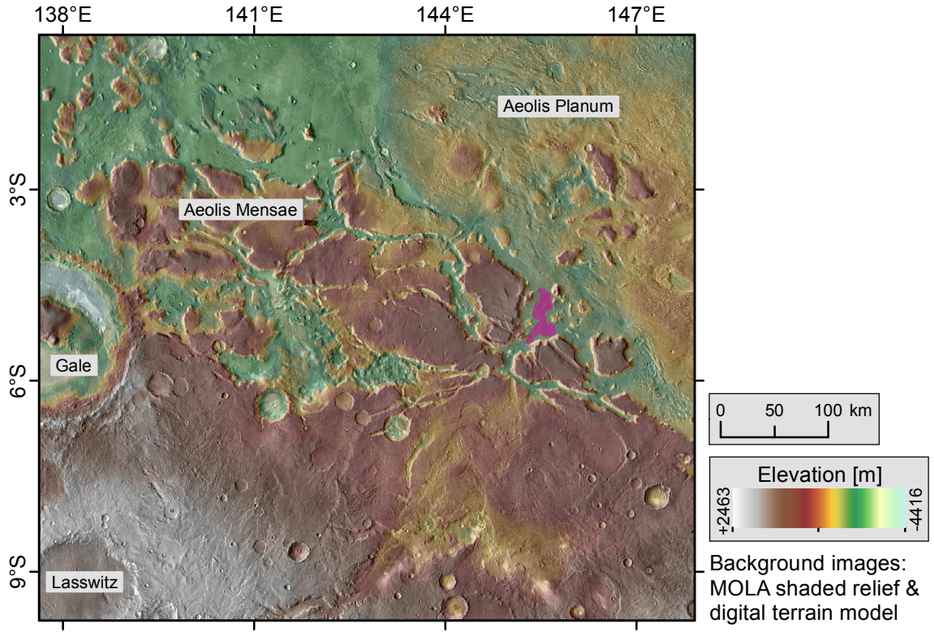

Crater counting area **3**

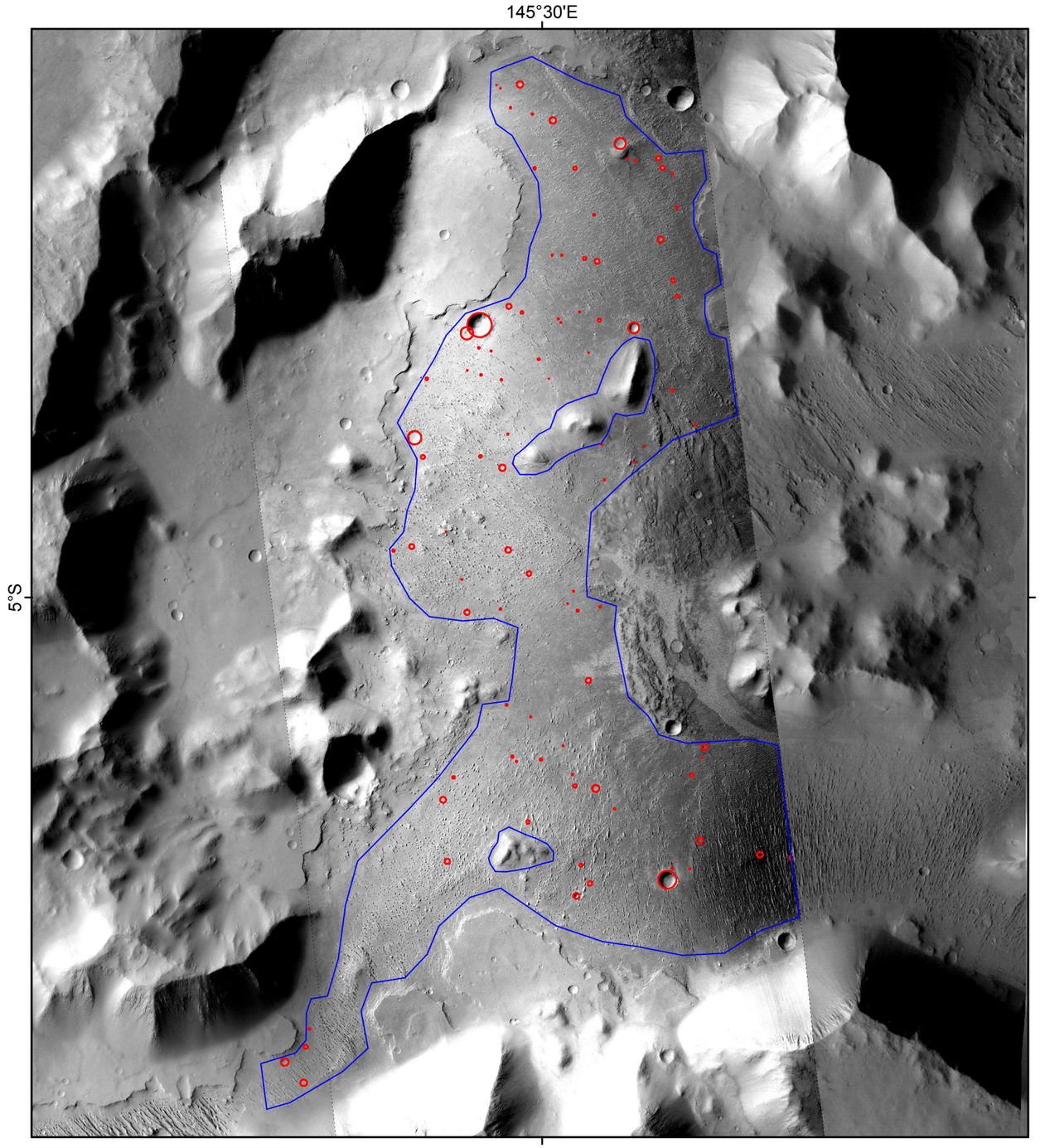

Projection: Equidistant Cylindrical
Datum: Mars sphere
Central Meridian: 0.0000
Standard Parallel 1: 0.0000
Units: Meter

Crater model age(s)

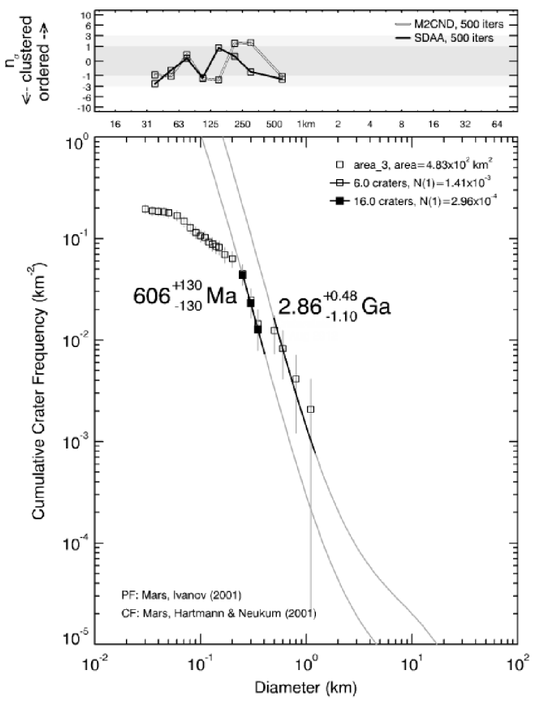

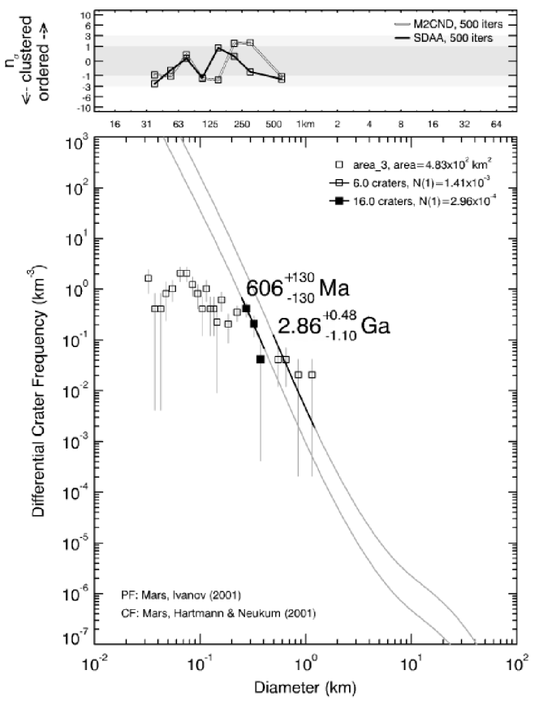

Regional context

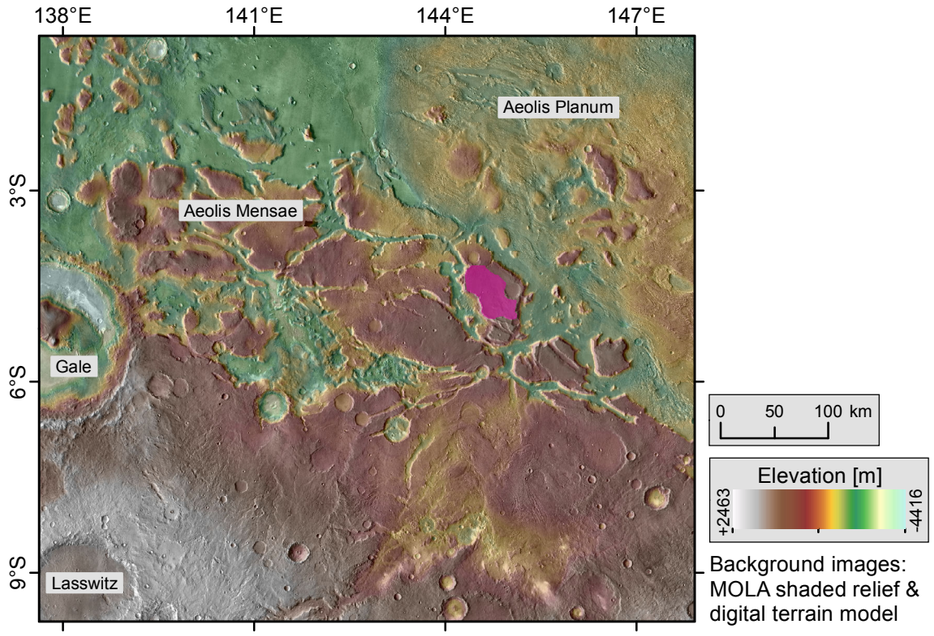

Background images:
MOLA shaded relief &
digital terrain model

Crater model age(s)

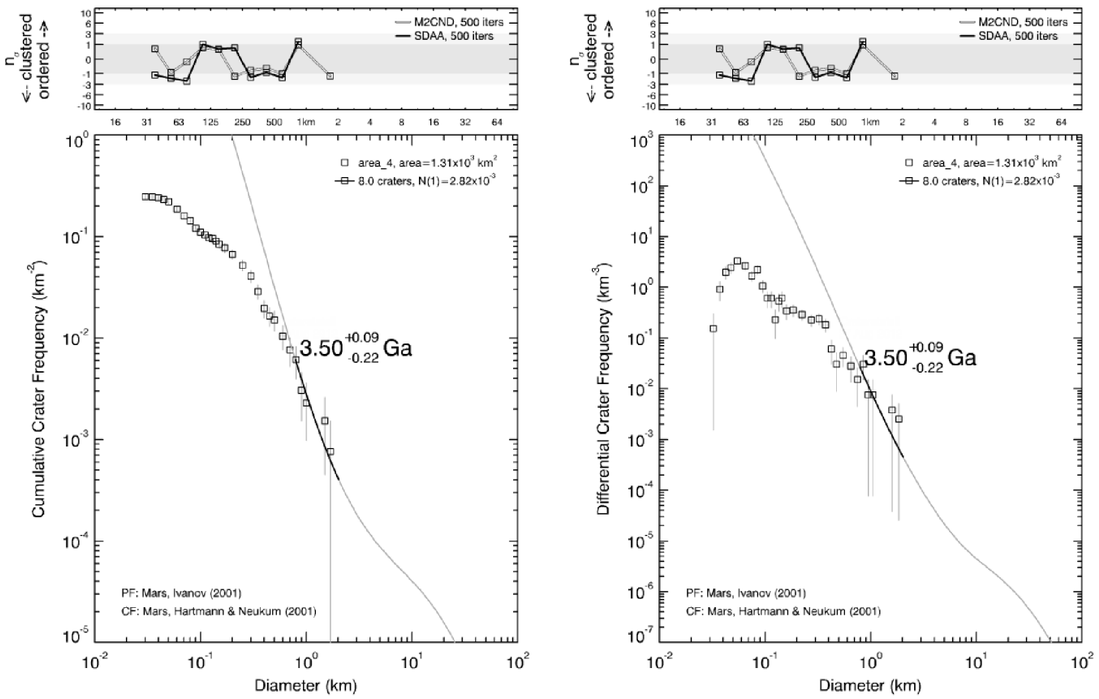

Crater counting area **4**

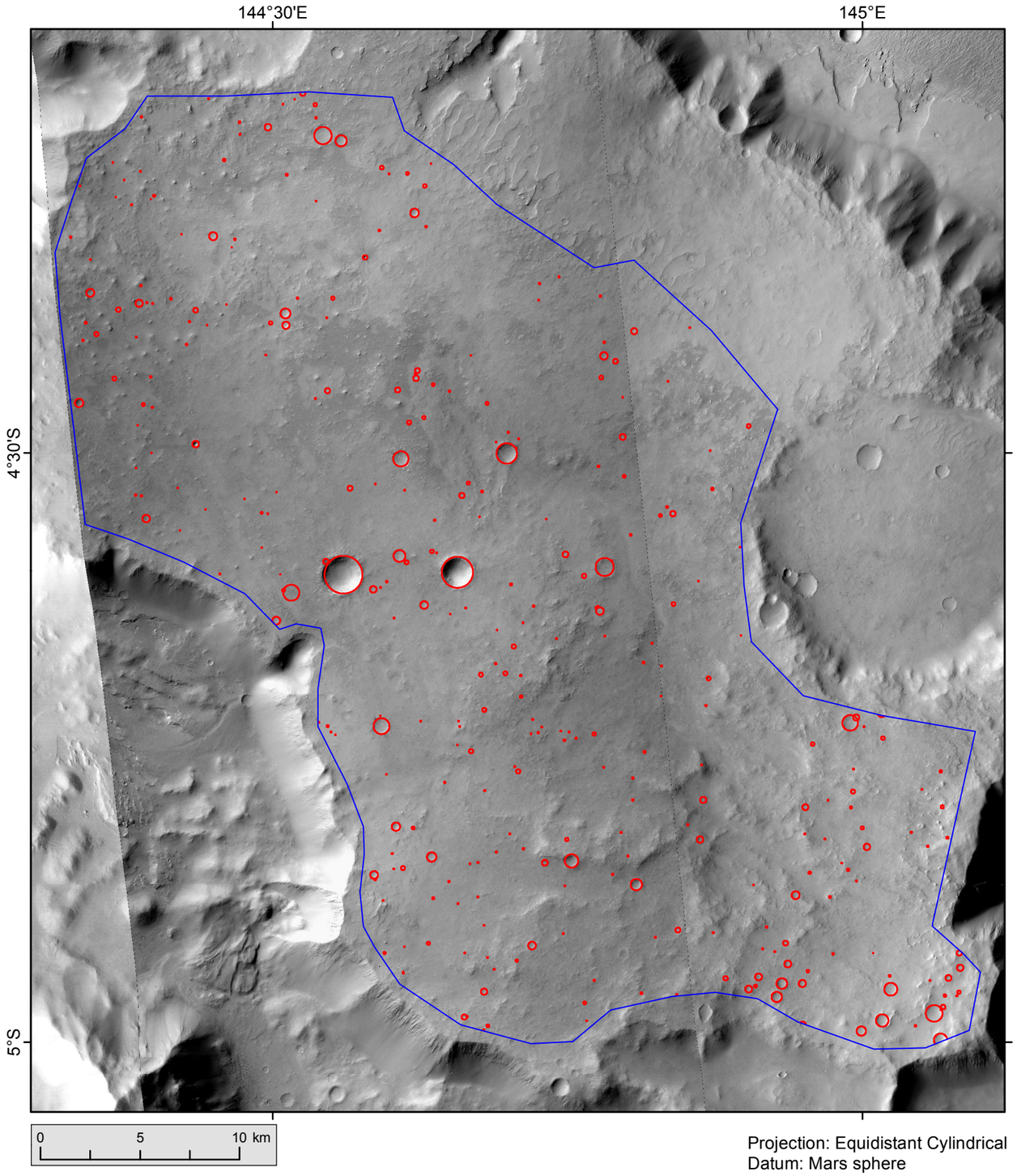

Projection: Equidistant Cylindrical
Datum: Mars sphere
Central Meridian: 0.0000
Standard Parallel 1: 0.0000
Units: Meter

Regional context

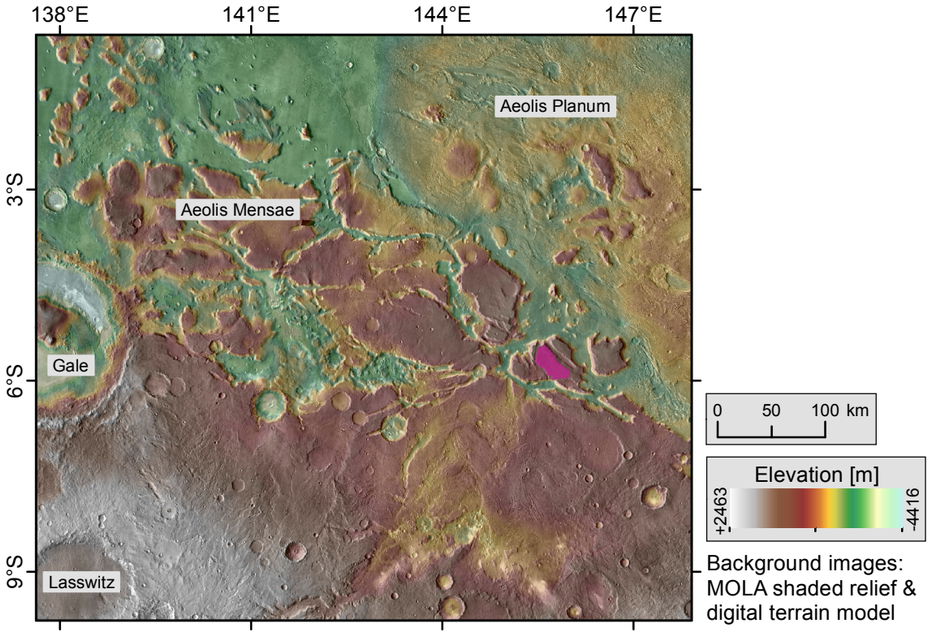

Crater counting area **5**

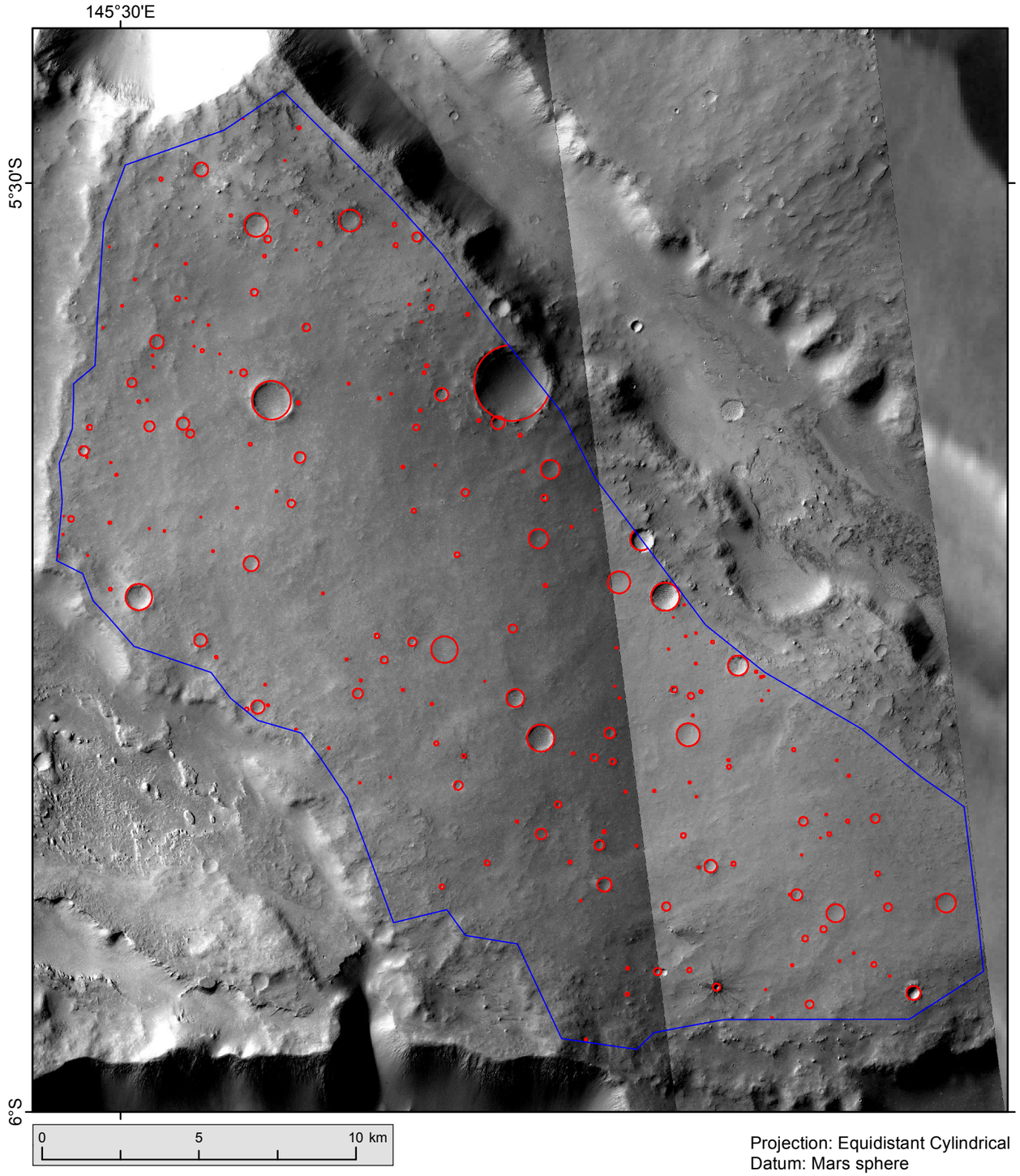

Projection: Equidistant Cylindrical
Datum: Mars sphere
Central Meridian: 0.0000
Standard Parallel 1: 0.0000
Units: Meter

Crater model age(s)

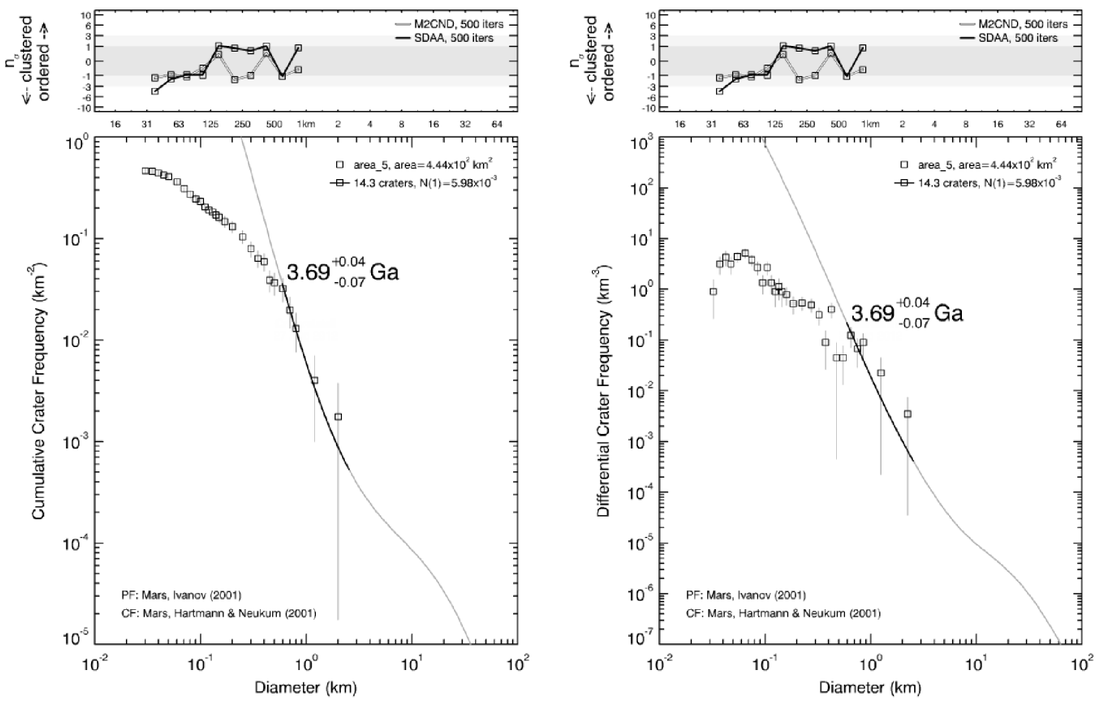

Regional context

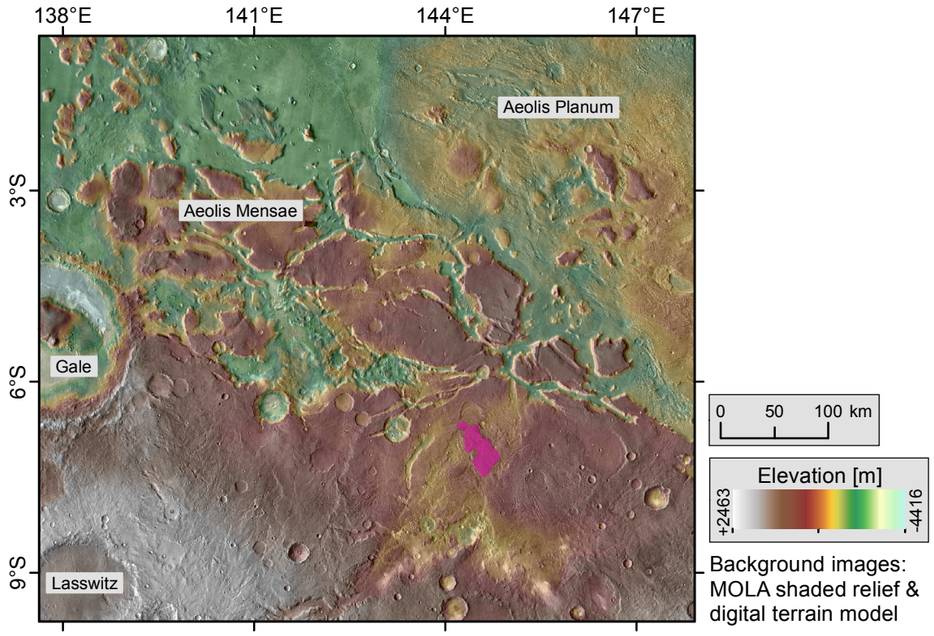

Crater counting area **6**

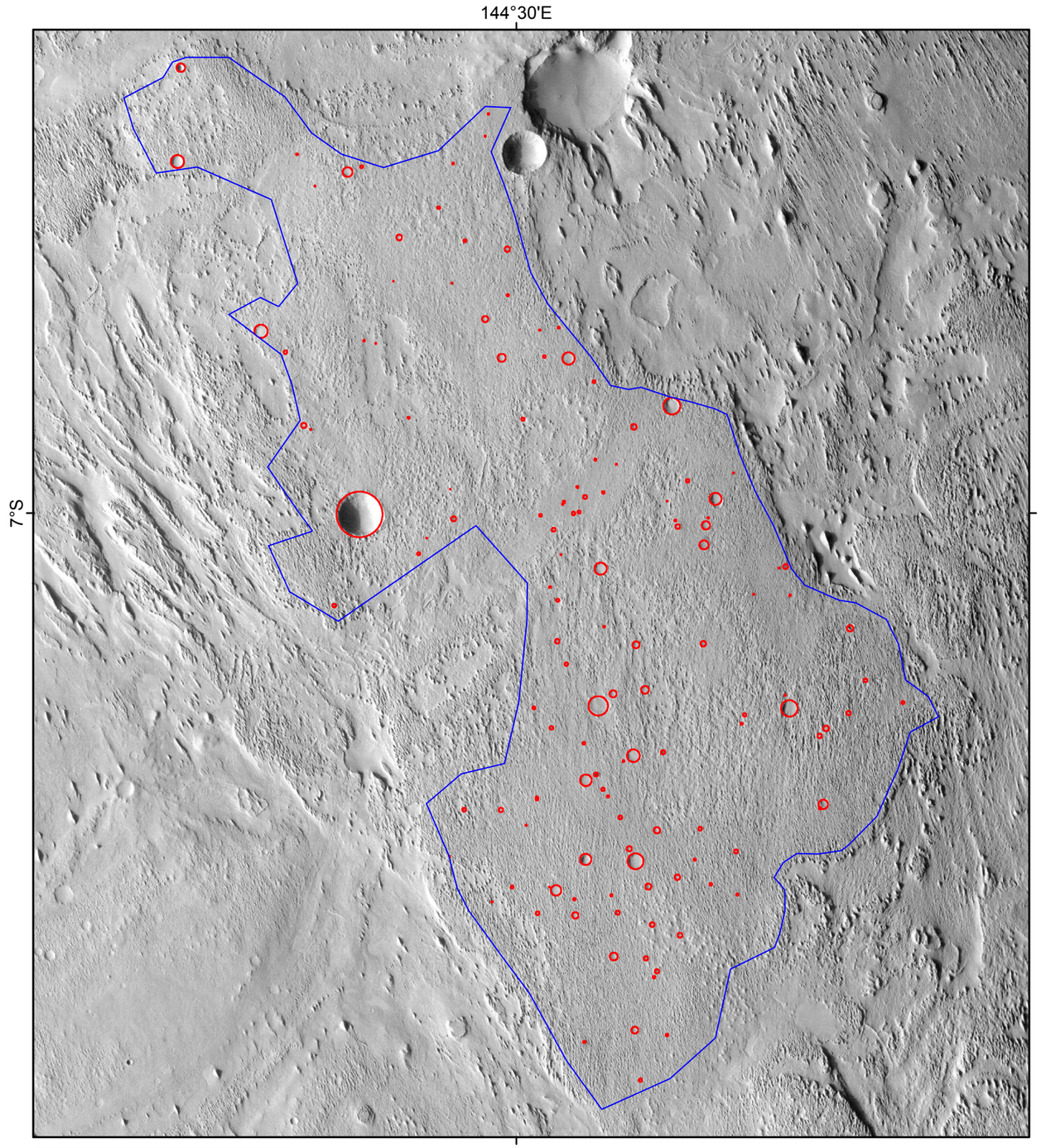

Crater model age(s)

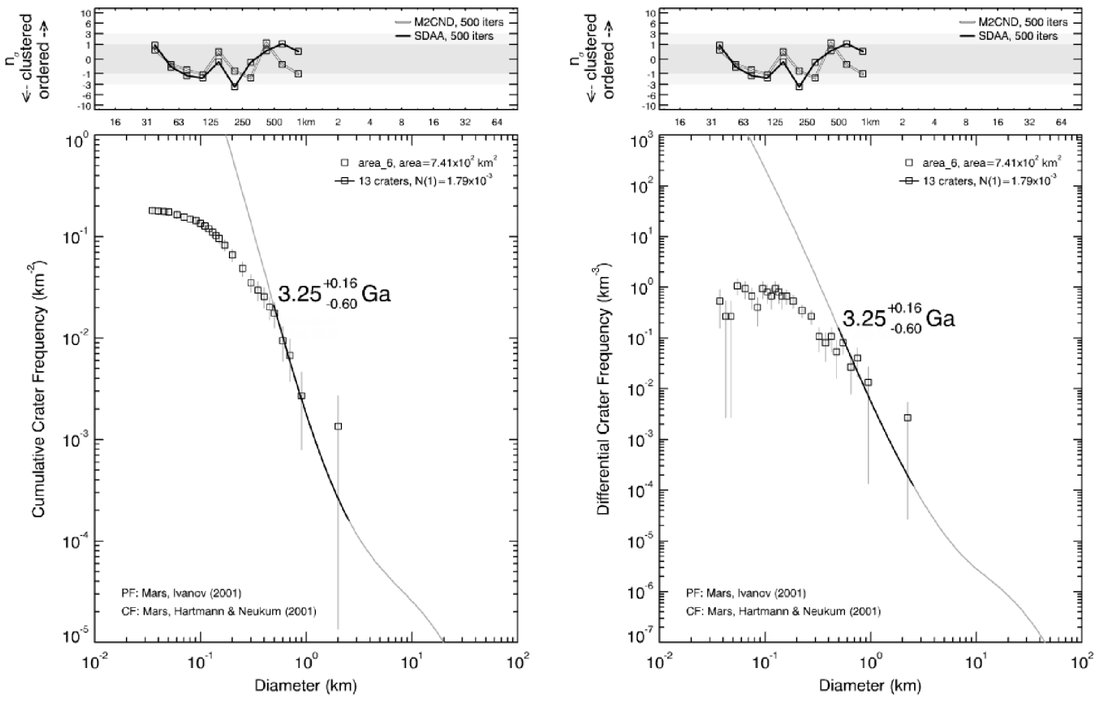

Regional context

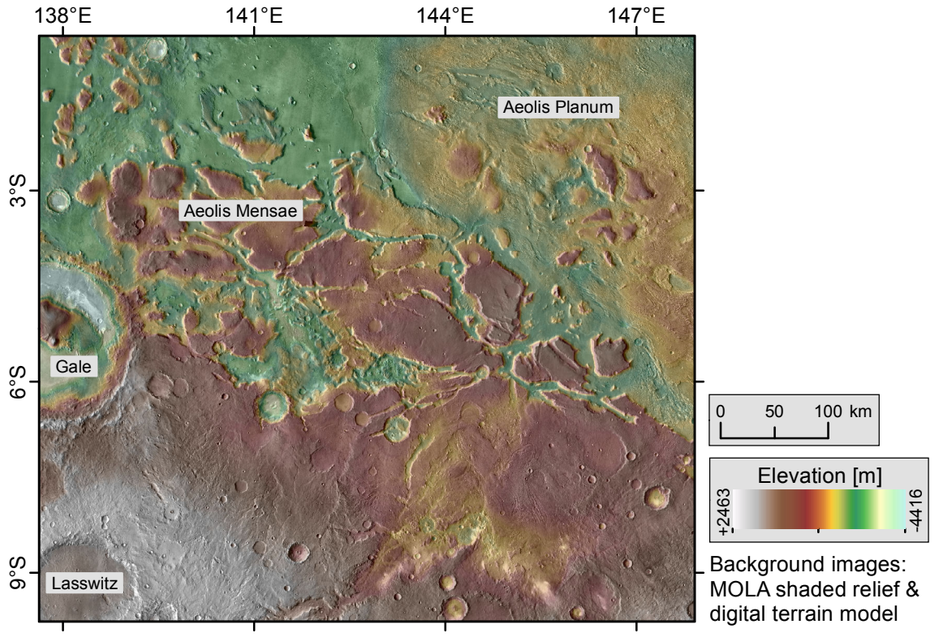

Crater counting area **7**

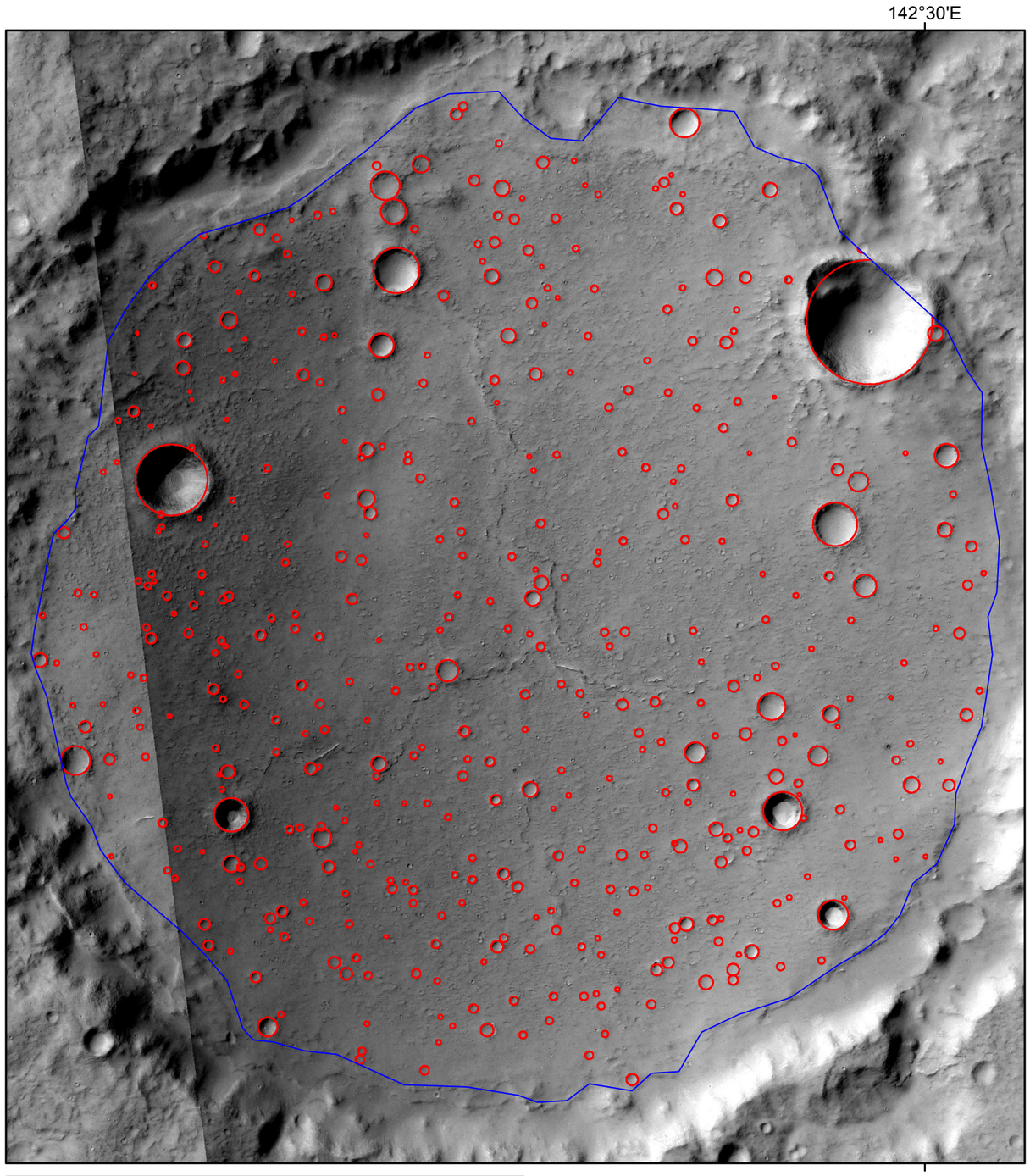

Crater model age(s)

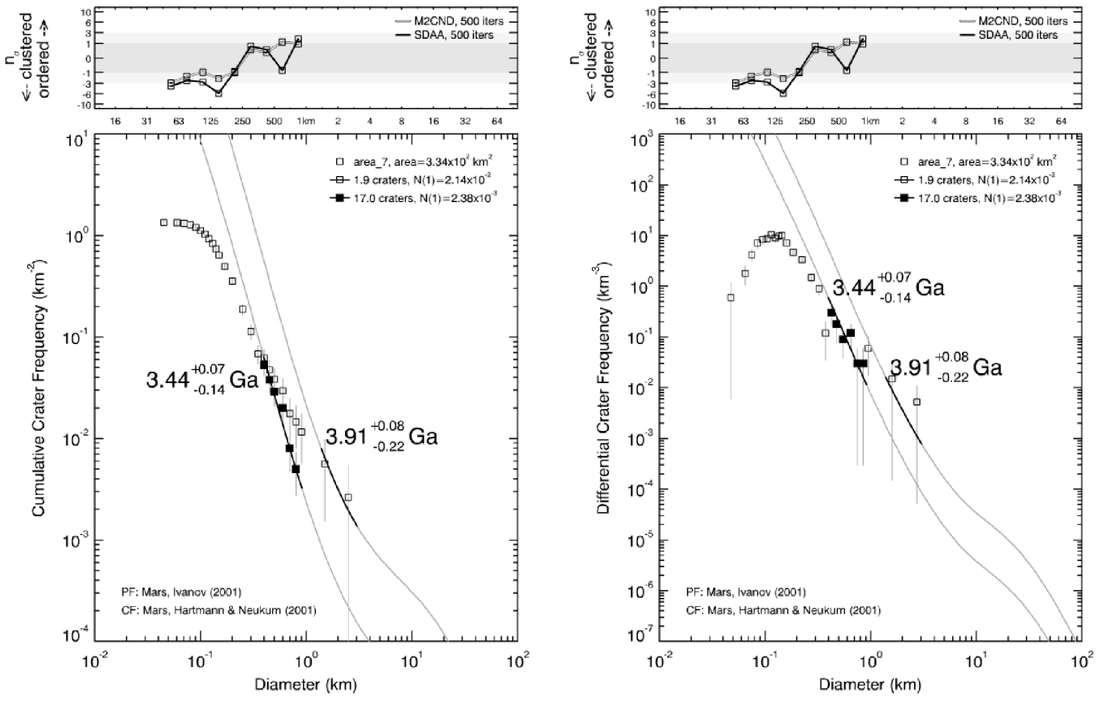

Table DR1: Detailed documentation of crater statistics for seven areas. Graphs and counting areas are portrayed on subsequent pages of the annex.

Description	Crater count ID	Coordinates[1] [°]		Area [km²]	Total no. craters	Resurfacing correction	D [km] in fit range		No. craters in fit range	Age[2] [Ga]					N_{cum}(1 km) /10^6 km² of fitted isochron(s)		Epoch[3]			Instrument	Image No.	Image Resolution [m/px]
		latitude	longitude East				D_{min}	D_{max}		best fit	error +	error -	max. fit	min. fit		error +/-	best fit	max. fit	min. fit			
Lobate feature	area_1	-7.77	145.16	1,625	61.7	no	1.2	2.5	4.9	3.68	0.072	0.15	3.75	3.53	5,630	2,530	eH	lN	lH	HRSC	h4136_0000.nd4.05, h4147_0000.nd4.07	12.5
Crater filling	area_2	-4.09 -4.04	141.68 141.52	45.91	118.2	no	0.15	0.3	11.9	0.633	0.18	0.18	0.813	0.453	308	88.6	mA	mA	mA	CTX	P05_002899_1759_XI_04S218W	5.26
Valley floor	area_3	-5.00	145.52	482.7	94.6	no	0.5	1.2	6	2.86	0.48	1.1	3.34	1.76	1,410	568	eA	eA	eA	CTX	P17_007593_1739_XN_06S214W	5.27
						yes	0.25	0.4	16	0.606	0.13	0.13	0.736	0.476	296	62.4	mA	mA	mA			
Top of mesa	area_4	-4.61	144.69	1,309	323.9	no	0.8	2	8	3.5	0.089	0.22	3.59	3.28	2,820	987	lH	lH	eA	CTX	P02_001844_1738_XN_06S214W, B22_018089_1764_XI_03S215W	5.26 5.37
						yes	0.35	0.6	24	0.802	0.13	0.13	0.932	0.672	391	63.1	mA	mA	mA			
Top of mesa	area_5	-5.73	145.69	444.4	206.6	no	0.6	2.5	14.3	3.69	0.045	0.066	3.74	3.62	5,980	1,560	eH	eH	lH	CTX	P17_007593_1739_XN_06S214W, B20_017456_1738_XN_06S214W	5.27 5.25
Lobate feature	area_6	-7.05	144.53	741.3	134	no	0.5	2.5	13	3.25	0.16	0.6	3.41	2.65	1,790	490	eA	eA	eA	CTX	B01_010019_1722_XI_07S215W, B07_012287_1722_XI_07S215W	5.25 5.22
Crater filling	area_7	-10.25	142.36	334.1	448	no	1.4	3	1.9	3.91	0.084	0.22	3.99	3.69	21,400	15,500	mN	eN	eH	CTX	B16_015887_1704_XN_09S217W, B17_016454_1696_XN_10S217W	5.21 5.15
						yes	0.4	0.9	17	3.44	0.075	0.14	3.52	3.3	2,380	515	eA	lH	eA			

[1] Centre coordinates of counting area; multiple coordinates mean multiple subareas.

[2] Crater model ages were determined using the Ivanov (2001) production function and the Hartmann and Neukum (2001) chronology function.

[3] Epoch boundaries after Werner and Tanaka (2011); N (Noachian), H (Hesperian), A (amazonian); e (Early), m (Middle), l (Late).

Table DR2: Quantification of the likelihood of glacial overdeepening of valleys in the Aeolis Mensae region as reflected in power functions of half-valley cross sections and second-order polynomial functions fitted to entire cross-sections, excluding convex shoulders (see Figure 3), alongside values for glacial troughs on Earth.

	Location (Lat/Long)	*Power function exponent (*b*-value) fitted to half-valley cross section (and R^2)	R^2 of second order polynomial fitted to entire valley cross section
Mars T1	3.8º S / 141.8º E	1.89 (0.963)	0.972
Mars T2	4.4º S / 142.0º E	1.66 (0.933)	0.968
Mars T3	3.8º S / 140.3º E	1.97 (0.955)	0.992
Mars T4	4.5º S / 143.8º E	1.91 (0.900)	0.970
Mars T5	3.6º S / 143.8º E	1.89 (0.953)	0.964
Mars T6	3.1º S / 141.8º E	2.19 (0.933)	0.994
Mars T7	5.6º S / 140.0º E	2.07 (0.856)	0.961
Mars T8	5.6º S / 140.7º E	1.60 (0.989)	0.974
Mars T9	6.2º S / 145.8º E	2.46 (0.936)	0.972
Mars T10	6.5º S / 146.5º E	1.96 (0.972)	0.952
Mars T11	2.9º S / 132.4º E	1.75 (0.944)	0.995
Mars T12	0.0º / 125.6º E	1.49 (0.911)	0.966
Mars T13	2.0º N / 121.2º E	1.84 (0.946)	0.922
Earth	Sierra Nevada, USA (James, 1996)	1.15 to 3.3 (non-stepped profiles)	0.623 to 0.996
Earth	British Columbia, Canada (Evans, 2007)	n/a	0.951 to 0.974
Earth	Wastwater, UK (Evans, 2007)	n/a	0.997
Earth	Beartooth Mountains USA (Graf, 1970)	1.63 to 1.84	n/a
Earth	Lapporten, Sweden (Svensson, 1959)	2.05 to 2.18	n/a
Earth	Tian Shan, China (Li et al., 2001)	1.03 to 3.50	0.871 to 0.997
Theoretical	Numerical modeling of glacial erosion (Harbor, 1992)	2.22 to 2.32 (approx 'steady-state' valley form)	n/a

*Power-law curves were fitted to half-valley cross-profiles with the origin defined as the lowest point in the valley (see Harbor and Wheeler, 1992).